Fabrication and photocatalytic characterizations of ordered nanoporous X-doped (X = N, C, S, Ru, Te, and Si) TiO2/Al2O3 films on ITO/glass

ARTICLE *in* LANGMUIR · SEPTEMBER 2005

Impact Factor: 4.46 · DOI: 10.1021/la050902j · Source: PubMed

5 AUTHORS, INCLUDING:

Song-Zhu Kure-Chu
Iwate University
48 PUBLICATIONS **1,267** CITATIONS

SEE PROFILE

Fabrication and Photocatalytic Characterizations of Ordered Nanoporous X-Doped (X = N, C, S, Ru, Te, and Si) TiO_2/Al_2O_3 Films on ITO/Glass

Song-Zhu Chu,*,† Satoru Inoue,† Kenji Wada,† Di Li,† and Jun Suzuki‡

Advanced Materials Laboratory, National Institute for Materials Science (NIMS), Namiki 1-1, Tsukuba, Ibaraki 305-0044, Japan, and Kaken Company Limited, Hori-Machi, Mido, Ibaraki 310-0903, Japan

Received April 6, 2005. In Final Form: June 22, 2005

Transparent, ordered nanoporous TiO_2/Al_2O_3 composite films doped with metal elements (Ru, Si, and Te) and nonmetal elements (N, C, and S) were fabricated by successive anodization and sol−gel process directly on glass substrates covered with a tin-doped indium oxide (ITO) film. The doping of ruthenium, nitrogen, carbon, and sulfur in TiO_2 exhibited an enhanced effect on the absorbance, while the doping of silicon and tellurium showed little effect. Particularly, the N- and Ru-doped TiO_2/Al_2O_3 films on ITO/glass developed an enhanced absorption red shift of 580 nm (−N) and 500 nm (−Ru). The nanoporous TiO_2/Al_2O_3 composite film exhibited the highest photocatalytic activity in decomposing acetaldehyde under ultraviolet-light irradiation, with a value of 13 times in initial reaction rate or 7.8 times in quantum yield higher than a commercially available TiO_2 material, Degussa P25. The ultraviolet-light photocatalytic activities of nanoporous TiO_2/Al_2O_3 films were enhanced by the doping of nitrogen, carbon, and sulfur but slightly weakened by the doping of ruthenium, silicon, and tellurium. Particularly, the nanoporous N-doped TiO_2/Al_2O_3 films exhibited effective photocatalytic activity on ultraviolet light decomposition of a highly toxic dioxin, HpCDD, and gave the highest decomposition rate of ∼95% (via 7 h of irradiation) for the specimen with a dopant content of 1.7 wt % nitrogen.

1. Introduction

Nanoporous TiO_2 materials have attracted great attention because of widely potential applications in electronic, photoelectrochemical, and photocatalytic systems such as photoelectrodes,[1−3] photoelectrochemical solar cells,[4−6] gas sensors,[7−9] and high-performance photocatalysts.[10−12] Thus far, many studies have been conducted on the preparation of various porous TiO_2 nanomaterials, including nanoporous films and nanotubule arrays, by sol−gel process,[10−14] anodization,[9,15,16] and electrodeposition.[17,18] Among the methods mentioned above, the sol−gel process combined with some template techniques (e.g., upon porous alumina) is the most intriguing because of the arbitrary controlling of porous morphology by templates and TiO_2 composition through solutions for sol−gel coating. Especially, fabricating porous TiO_2 nanostructures with uniform morphology and improved properties directly on mechanically strong substrates is necessary and of technical significance for various practical applications.

As a well-known optoelectronic semiconductor with photoelectrochemical and photocatalytic activity, TiO_2 is considered to be an effective and nontoxic photocatalyst for atmosphere cleaning and water purification. Many studies had been devoted to the mechanism and the relation to the particle sizes in photocatalytic reactions on TiO_2.[1,19−23] Recently, to enhance or improve the photocatalysis from ultraviolet ($300 < \lambda < 400$ nm) to visible light range ($\lambda > 400$ nm), many studies on the substitutional doping of metal ions (e.g., Fe,[24,25] Co,[26]

* To whom correspondence should be addressed: Materials Science Research Lab., Central Research Institute of Electric Power Industry (CRIEPI), Nagasaka 2-6-1, Yokosuka, Knagawa, 240-0196, Japan. E-mail: chusongz@criepi.denken.or.jp. Telephone: +81-46-856-2121. Fax: +81-46-856-5571.

† National Institute for Materials Science (NIMS).

‡ Kaken Co. Ltd.

(1) Fujishima, A.; Honda, K. *Nature* **1972**, *37*, 238.
(2) O'Regan, B.; Grätzel, M. *Nature* **1991**, *353*, 737.
(3) Ma, T. L.; Inoue, K.; Noma, H.; Yao, K.; Abe, E. *J. Photochem. Photobio., A* **2002**, *152*, 207.
(4) O'Regan, B.; Schwartz, D. T.; Zakeeruddin, S. M.; Gratzel, M. *Adv. Mater.* **2000**, *12*, 1263.
(5) Zhang, D. S.; Yoshida, T.; Minoura, H. *Chem. Lett.* **2002**, *9*, 874.
(6) Bisquert, J.; Zaban, A.; Salvador, P. *J. Phys. Chem. B* **2002**, *106*, 8774.
(7) Fujishima, A.; Rao, N. T.; Tryk, D. A. *Electrochim. Acta* **2000**, *45*, 4683.
(8) Hoyer, P.; Masuda, H. *J. Mater. Sci. Lett.* **1996**, *15*, 1228.
(9) Mor, G. K.; Carvalho, M. A.; Varghese, O. K.; Pishko, M. V.; Grimes, C. A. *J. Mater. Res.* **2004**, *19*, 628.
(10) Lakshmi, B. B.; Dorhout, P. K.; Martin, C. R. *Chem. Mater.* **1997**, *9*, 857.
(11) Chu, S. Z.; Wada, K.; Inoue, S.; Todoroki, S. *Chem. Mater.* **2002**, *14*, 266.
(12) Chu, S. Z.; Wada, K.; Inoue, S. *Adv. Mater.* **2002**, *23*, 1752.
(13) Chu, S. Z.; Wada, K.; Inoue, S.; Todoroki, S. *J. Electrom. Soc.* **2002**, *149*, B321.
(14) Meng, Q. B.; Fu, C. H.; Einaga, Y.; Gu, Z. Z.; Fujishima, A.; Sato, O. *Chem. Mater.* **2002**, *14*, 83.
(15) Miller, D.; Mamiche-Afara, S.; Dignam, M. J.; Moskovits, M. *Chem. Phys. Lett.* **1983**, *100*, 236.
(16) Chu, S. Z.; Inoue, S.; Wada, K.; Hishita, S.; Kurashima, K. *J. Electrochem. Soc.* **2005**, *152*, B116.
(17) Ishikawa, Y.; Matsumoto, Y. *Electrochim. Acta* **2001**, *46*, 2819.
(18) Peiró, M.; Brillas, E.; Peral, J.; Domènech, X.; Ayllón, J. A. *J. Mater. Chem.* **2002**, *12*, 2769.
(19) Sopyan, I.; Watanabe, M.; Murasawa, S.; Hashimoto, K.; Fujishima, A. *J. Photochem. Photobio., A* **1996**, *98*, 79.
(20) Kawai, T.; Sakata, T. *Nature* **1980**, *286*, 474.
(21) Zhnag, Z.; Wang, C. C.; Zakaria, R.; Ying, J. Y. *J. Phys. Chem. B* **1998**, *102*, 10871.
(22) Almquist, C. B.; Biswas, P. *J. Catal.* **2002**, *212*, 145.
(23) Addamo, M.; Augugliaro, V.; Paola, A. D.; García-López, E.; Loddo, V.; Marcì, G.; Molinari, R.; Palmisano, L.; Schiavello, M. *J. Phys. Chem. B* **2004**, *108*, 3303.
(24) Zhang, Y. H.; Ebbinghaus, S. G.; Weidenkaff, A. *Chem. Mater.* **2003**, *15*, 4028.
(25) Wang, C. Y.; Bottcher, C.; Bahnemann, D. W.; Dohrmann, J. K. *J. Mater. Chem.* **2003**, *13*, 2322.
(26) Iwasaki, M.; Hara, M.; Kawada, H.; Tada, H.; Ito, S. *J. Colloid Interface Sci.* **2000**, *224*, 202.

10.1021/la050902j CCC: $30.25
Published on Web 07/20/2005

La,[27,28] Ru,[29] Zr,[30] Nd,[31] and Si[32]) and nonmetallic elements (N,[33−35] S,[36] and C[37]) have been intensely investigated on the TiO_2 system. It is commonly recognized that the doping in TiO_2 improves the photocatalytic activity by shifting the onset of the response from the ultraviolet to the visible light range. Among the dopants mentioned above, N-doped TiO_2 is the most effective and has been elaborated in many theoretical and experimental studies, in which a widely acceptable explanation is a band-cap narrowing effect because of the substitution of nitrogen from oxygen, thus leading to the photocatalytic reaction under the visible light with low energy. In contrast, it is usually considered that the metal doping to the photocatalytic improvement of TiO_2 lies in the shifting of light absorption toward the visible region, accompanying with the by effects of the undesired instability because of the lattice distortion or bond weakening and to the increased carrier trapping from the formation of electronic mid-gap states associated doping elements.

In our previous studies,[38,39] we had reported the fabrication of highly porous TiO_2/Al_2O_3 composite nanostructures on Ti/glass substrates by successive anodization and sol−gel process and found that high photocatalytic activities were achieved in decomposing acetaldehyde under ultraviolet light irradiation. In the present paper, we mainly report the fabrication of various transparent, doped nanoporous TiO_2/Al_2O_3 composite films on ITO/glass by an analogous method to the previous approach and further explore the photocatalytic activities in decomposing acetaldehyde and highly toxic dioxins under ultraviolet light irradiation.

2. Experimental Procedures

2.1. Fabrication Process. The synthetic method of nanoporous TiO_2-based films on glass substrates was similar to previous studies.[11,12] Briefly, a high-purity aluminum layer (99.99%, ≈1.5 μm thick) was deposited on a glass substrate (soda lime glass, 25 × 100 × 0.7 mm) covered with a tin-doped indium oxide film (ITO, ≈120 nm, ≈10 Ω in sheet resistance) by multicycled radio frequency (RF) sputtering at a rate of 1.5 nm/s. To form nanoporous alumina films, the Al/ITO/glass specimens were anodically oxidized in a 10 vol % H_3PO_4 solution at a constant potential of 130 V and 4 °C, until the aluminum layers were completely transformed into alumina (characterized by the anodic current dropping from 20 to 30 to ≈3 A/m^2 and by the appearance changing from opaque to transparent).[13] Then, the specimens were immersed in a 5 vol % H_3PO_4 solution at 30 °C for 45 min to enlarge the pores for the easy filling of various TiO_2-based solutions in the successive sol−gel process. The sol−gel process was performed by one-step dip coating, in which various TiO_2-based oxides were coated on pore walls of the alumina films, to form various porous TiO_2/Al_2O_3 composite nanostructures on ITO/glass with open apertures. On the basis of the results of a previous study,[39] the sol−gel-coated specimens were consecutively heated at 100 °C for 1 h and 500 °C for 2 h, to achieve highly crystalline anatase phase for high photocatalytic activity. Other details on the coating conditions in the sol−gel process were the same as in a previous study.[11]

2.2. Photocatalysts Synthesis. All of the solutions for anodization, pore-widening, and sol−gel coating were prepared by analytical-grade reagents as received (Kanto Chem. Co.). The precursory TiO_2 solution (≈5 wt %, solution A) used in the sol−gel process was prepared with titanium isopropoxide, acetylacetone, distilled water, and ethanol in a mole ratio of 1:1.1:3:20.[11] In the sol−gel coating, the precursory TiO_2 solution was diluted with ethanol into a 3 wt % solution (solution B; viscosity ≈ 1.76 cSt; 20 °C), to achieve a continuous TiO_2 coating and a hollow-type composite nanostructure with open apertures by one-step dip coating. The Ru-doped TiO_2 solutions were prepared by adding a mixed solution (2 g/L $RuCl_3 \cdot H_2O$ + 3 vol % H_2O_2) in solution B for a dopant concentration of 2−4 wt % in RuO_2. The N-doped TiO_2 solution was prepared by adding a 1 M NH_3NO_3 solution in solution B to achieve nitrogen contents of 1−4 wt %. The NCS-doped TiO_2 solution was prepared by adding 1 M thiourea solution in solution B to obtain 4.32 wt % NCS in TiO_2 or 1.65, 0.72, and 1.86 wt % as N, C, and S elements, respectively. The Si,Te-doped TiO_2 solution was prepared by adding a mixed (SiO_2 + 2.5% TeO_2) solution in solution A to achieve a thick coating for robust TiO_2−4% SiO_2−1% SiO_2 nanotubule arrays on glass.[12] Except for the Ru-doped TiO_2 solution, which was dark red, all of the other TiO_2 solutions were transparent with a bright yellow color.

2.3. Characterizations. The morphology of the specimens was observed by a field emission scanning electron microscope (FESEM, S-5000, Hitachi) after coating with a thin osmium film. The crystallographic structures of the specimens were analyzed by an X-ray diffractometer (XRD, RINT-2200V/PC, CuKα, 40 kV/40 mA) and a transmission electron microscope (TEM, JEOL-200 kV). For the TEM observation, the TiO_2/Al_2O_3 layer stripped from the substrate was embedded into epoxy resin and cut by an ultramicrotome (LKB-2088/V) with a diamond knife into ∼60 nm thick slices. The sliced samples were then set on carbon-coated copper microgrids and observed in the bright field along with the corresponding diffraction pattern. The transparency of the specimens was investigated by an UV−vis spectrometer (U-3500, Hitachi).

2.4. Photocatalytic Measurements. The photocatalytic activities of the various TiO_2-based nanostructures on ITO/glass were evaluated by photodecomposition tests of the following substances under ultraviolet light irradiation.

(a) Acetaldehyde Gas. The photocatalytic decomposition test was carried out in a closed circulation system (CCS; 250 cm^3) interfaced to a gas chromatograph (Hitachi, G-35A) with a thermal conductor detector (TCD) and a photoionization detector (PID) for acetaldehyde and CO_2 analysis, respectively. Prior to the catalytic experiments, the specimens were treated in a flow of oxygen gas at 300 °C until no CO_2 product was detected. The specimens were then separated from the flow system and switched to the CCS by two three-way stopcocks and evacuated under a vacuum of 10^{-5} Pa and 300 °C for 1 h. After the specimens had cooled to room temperature, the reactant, a gaseous mixture of 93.3 kPa CH_3CHO−He (930 ppm) and 13.3 kPa O_2, was introduced in the reactor. The nanoporous specimens (≈1 × 1 cm) were irradiated from the outside of the reactor by a 200 W Hg−Xe lamp (Hayashi, LA300UV-1, $\lambda = 365$ nm) with an incident light intensity of 50 mW/cm^2. For reference, 30 mg of commercial TiO_2 powder (Degussa P25, 50 m^2/g) was put on a ϕ1.3-cm dent on glass and irradiated under the same conditions.

(b) Dioxin Solution. The reactant was a standard dioxin solution [1,2,3,4,6,7,8-heptachlorodibenzo-*p*-dioxin (HpCDD), 50 μg/L in toluene]. The HpCDD is a highly toxic and cancer-induced substance, with a toxic equivalency factor (TEF) of 0.01 [world health organization (WHO), 1998]. In the experiment, 0.20-mL of HpCDD solution was dropped onto the nanoporous TiO_2-coated specimens (≈2 × 4 cm) on a hotplate and dried by Ar gas flow in the dark. The samples with dried HpCDD (≈10 μg) were then set in the reactor of a closed circulation system (110 cm^3) and irradiated inside the reactor by two 8 W black light lamps

(27) Jing, L. Q.; Sun, X. J.; Xin, B. F.; Wang, B. Q.; Cai, B. Q.; Fu, H. G. *J. Solid State Chem.* **2004**, *177*, 3375.
(28) Wei, H. Y.; Wu, Y. S.; Lun, N.; Zhao, F. *J. Mater. Sci.* **2004**, *39*, 1305.
(29) Ohno, T.; Tanigawa, F.; Fujihara, K.; Izumi, S.; Matsumura, M. *J. Photochem. Photobio., A* **1999**, *127*, 107.
(30) Wang, Y. M.; Liu, S. W.; Wang, S. F.; Gu, F.; Gai, X. Z.; Cui, X. X.; Pan, J. *J. Mol. Catal. A: Chem.* **2004**, *215*, 137.
(31) Hou, M. F.; Li, F. B.; Li, R. F.; Wan, H. F.; Zhou, G. Y.; Xie, K. C. *J. Rare Ear.* **2004**, *22*, 542.
(32) Takabayashi, S.; Nakamura, R.; Nakato, Y. *J. Photochem. Photobio., A* **2004**, *166*, 107.
(33) Asahi, R.; Morikawa, T.; Ohwaki, T.; Aoki, K.; Taga, Y. *Science* **2001**, *293*, 269.
(34) Premkumar, J. *Chem. Mater.* **2004**, *16*, 3980.
(35) Nakamura, R.; Tanaka, T.; Nakato, Y. *J. Phys. Chem. B* **2004**, *108*, 10617.
(36) Ohno, T.; Mitsui, T.; Matsumura, M. *Chem. Lett.* **2003**, *32*, 364.
(37) Eliseev, A. A. *MRS Bull.* **2004**, *29*, 4.
(38) Chu, S. Z.; Inoue, S.; Wada, K.; Li, D.; Haneda, H. *J. Mater. Chem.* **2003**, *13*, 866.
(39) Chu, S. Z.; Inoue, S.; Wada, K.; Li, D.; Haneda, H. *J. Phys. Chem. B* **2003**, *107*, 6586.

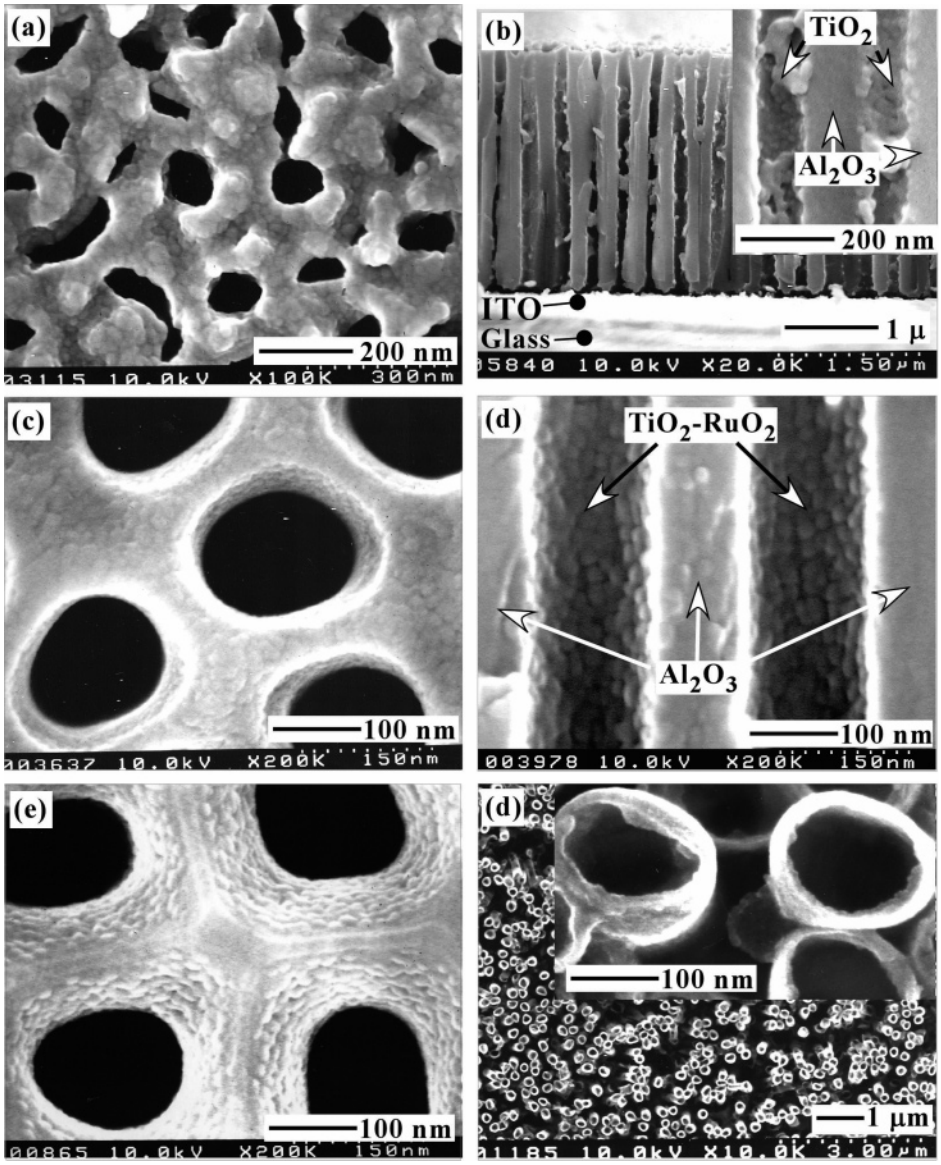

Figure 1. Field-emission scanning electron microscopic (FESEM) images of (a−e) various nanoporous TiO_2/Al_2O_3 composite films on ITO/glass coated with (a and b) pure TiO_2, (c and d) Ru-doped TiO_2, and (e) N-doped TiO_2, and (f) a $TiO_2-SiO_2-TeO_2$ nanotubule array after the removal of the anodic alumina.

[FL8BLB, λ_{max} = 360 nm (315−400 nm)] with a frontal light intensity of 0.9 mW/cm^2. The remnant HpCDD after irradiation was retrieved by immersing the irradiated samples in toluene in a circulated heating set at 70 °C for 3 h and then analyzed by GC−MS equipment (HP5890 II). The decomposition ratios were calculated from the deference between the original and the remnant HpCDD and corrected by the retrieving ratios of HpCDD without irradiation, which were close to 100%.

3. Results and Discussion

3.1. TiO_2-Based Nanostructures on ITO/Glass. Figure 1 shows the FESEM images of surface mophology and vertical fracture sections of various TiO_2-based composite films on ITO/glass. All of the porous nanostructures inherit the porous contours of the anodic alumina films (∼2.5 μm thick) with open apertures, composed of ordered straight nanopores of ϕ120−150 nm perpendicular to the substrates. The coatings on porous alumina films are dense and uniform, with a thickess of 20−30 nm. From the high-resolution images (parts a and b of Figure 1), the pristine TiO_2 coating without doping exhibits a rough surface consisting in clustered grains from 20 to 100 nm, because of a strong coagulation of the pure TiO_2 gel.[38] The Ru-doped TiO_2 coatings (parts c and d of Figure 1) show a relatively smooth surface composing of uniform grains ≈20 nm, indicating an inhibiting effect on the coagulation of the TiO_2 gel. The N-doped TiO_2 coatings (Figure 1e) exhibit a uniform granular texture similar to the Ru-doped TiO_2, irrespectively of the nitrogen content in TiO_2. While the addition of silicon and tellurium in TiO_2 leads to a dense coating with almost indiscernible gains (Figure 1f), because of the glassy nature of SiO_2 and TeO_2.[11]

As for appearance, all of the composite films are transparent (see Figures 4 and 5), with slight whitish, reddish, and yellowish colors for the TiO_2 ($-SiO_2-TeO_2$), Ru-doped TiO_2, and N-doped TiO_2 specimens, respectively. It was also found that the composite films did not crack or exfoliate when cutting or breaking the specimen, indicating the good adherence to the ITO/glass substrate and durable mechanical strength of the films. Moreover, from a Brunauer−Emmett−Teller (BET) measurement, the average ratio of the real surface areas of the composite films on glass to the apparent dimensions of the nanoporous samples was evaluated to be around 1.2 m^2/cm^2,

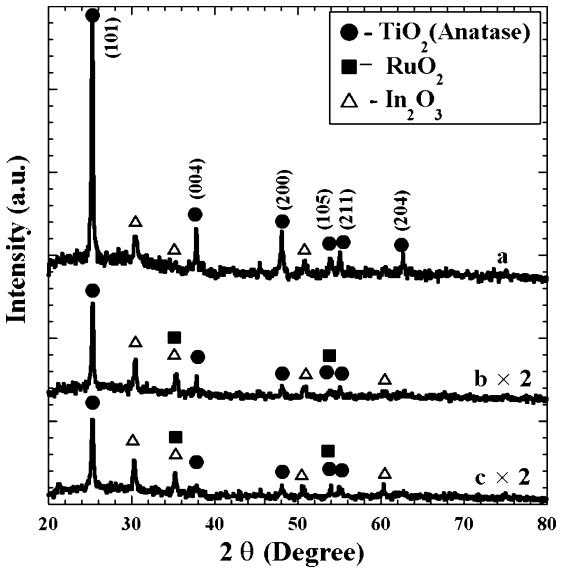

Figure 2. X-ray diffraction patterns of composite nanoporous films on ITO/glass coated with (a) pure TiO_2, (b) TiO_2−2% RuO_2, and (c) TiO_2−4% RuO_2.

which is an incomparably large surface area for other conventional filmy TiO_2 materials. In addition, according to the simulated calculation based on the surface FESEM images, the average porosities of the composite films were estimated to be 40−50%.

3.2. Crystallographic Structures. X-ray diffraction (XRD) analysis demonstrated that all of the TiO_2-based films mentioned above were well-crystallized after calcination at 500 °C for 2 h. The crystalline titanium oxides (Figure 2) are ascribed to polycrystalline tetragonal anatase with the lattice constants $a = 3.78$ Å and $c = 9.58$ Å [Joint Committee on Powder Diffraction Standards (JSPDS) card number 71-1168], which is well-known as a semiconductor with photoelectronic and photocatalytic activities. The intensities of the main peak (101) of anatase TiO_2 (Figure 2) for Ru-doped specimens were apparently lower than that of pure TiO_2, and the intensity decreased with the increase of Ru dopant, although they experienced the same sol−gel process. The Ru-doped TiO_2 specimens (parts b and c of Figure 2) show lower peak intensity than the pristine TiO_2 film (Figure 2a), and the peak intensity decreases with increasing ruthenium content, which is similar to the addition of Si and Te in TiO_2.[11] This indicates an inhibiting effect of Ru-doping on the crystalization of anatase TiO_2. Moreover, the Ru-doped TiO_2 specimens develop two small peaks at $2\theta = 35.1°$ and 54.3° (although it overlaped with indium oxide), which are close to the {101} and {211} reflections of tetragonal ruthenium oxide with the latttice constants $a = 4.49$ Å and $c = 3.11$ Å (JSPDS card number 71-2273). This infers that the ruthenium added in TiO_2 is over-dosed for doping and exists in independent oxide and a solid solution state in the lattice of the anatase TiO_2 matrix. In addition, it is was also found (not shown) that the doping of N, C, and S elements did not affect the crystal strutcure of TiO_2.

Figure 3 shows a representative vertical cross-sectional TEM image of the TiO_2/Al_2O_3 nanostructure. It is clearly seen that the TiO_2 layer between the alumina walls is composed of uniform nanocystals 10−20 nm in width. The TiO_2 cystals are closedly packed along the alumina pore walls, forming a continuous TiO_2 film in about three layers of nanocrystals (see the arrow in Figure 3). This indicates that the nodules of the TiO_2 layer in Figure 1b are secondary grains composing of numerous fine TiO_2

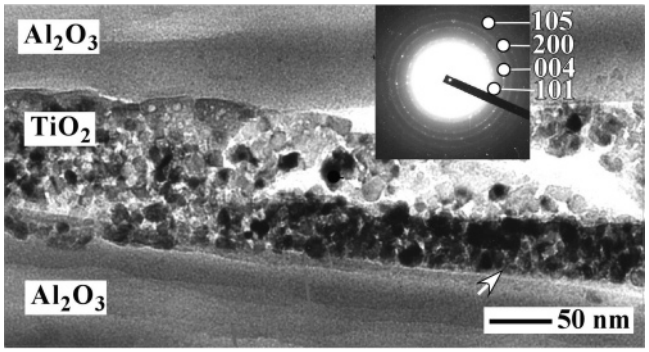

Figure 3. Representative transmission electron microscopic (TEM) image of the vertical cross section of TiO_2/Al_2O_3 composite film and the selected area electron diffraction (SAED) pattern corresponding to the TiO_2 region.

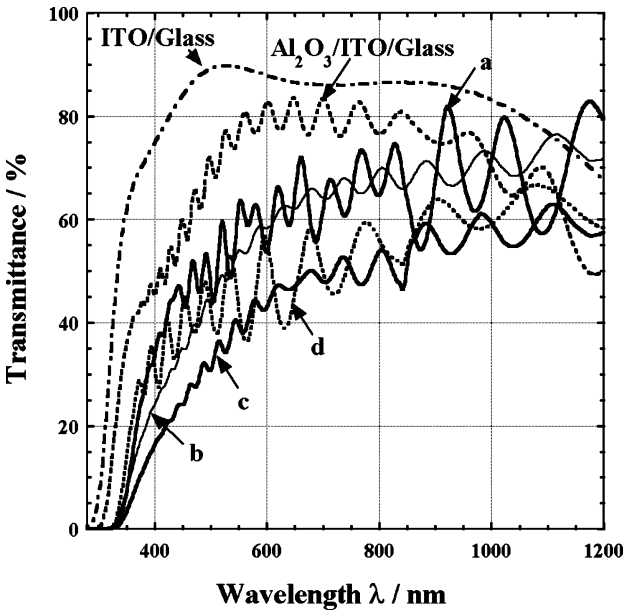

Figure 4. UV−vis transmission spectra of nanoporous films coated with (a) pure TiO_2, (b) TiO_2−2% RuO_2, (c) TiO_2−4% RuO_2, and (d) an integrated array of TiO_2−4% SiO_2−1% TeO_2 nanotubules on ITO/glass.

crystals. The selected area electron diffraction pattern corresponding to the TiO_2 layer (inset) displays several continuous rings that are close to the {101}, {004}, {200}, and {105} reflections of tetragonal anatase titanium oxide, which is consistent to the XRD results (Figure 2).

3.3. Transparency of Doped TiO_2/Al_2O_3 Films. The light absorption or transparency of TiO_2 materials is an important factor related to the efficiency of photocatalysis and other photochemical reactions. Figure 4 shows the UV−vis transmition spectra of various metal-doped TiO_2/Al_2O_3 composite nanostructures on ITO/glass substrates. For references, the specta of the ITO/glass substrate and the bared nanoporous alumina films on ITO/glass without sol−gel coating were also given in the figure. The TiO_2-based nanoporous films are moderately transparent throughout the UV and visible light regions, with lower transmittances than that of the bared nanoporous alumina film without sol−gel coating (···), indicating the stronger light absorbance of TiO_2-based films than the anodic alumina film. The pure TiO_2-coated nanoporous specimen (Figure 4a) exhibits a strong absorbance (transmittance ≈ 30%) near the wavelength of 387 nm, the bond cap of anatase TiO_2, and a high transmittance in the visible light range (50−70%). The doping of ruthenium in TiO_2 (parts b and c of Figure 4) leads to the enhancement of light

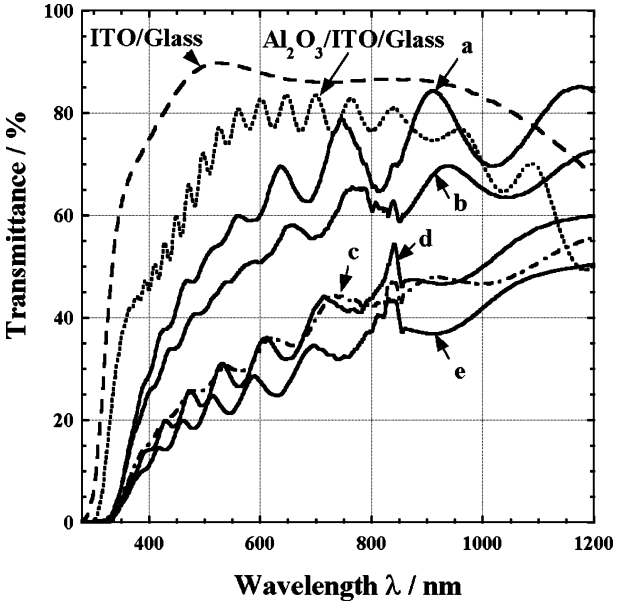

Figure 5. UV−vis transmission spectra of various nanoporous N-doped TiO_2/Al_2O_3 films on ITO/glass with dopant contents of (a) 0% N (i.e., pure TiO_2), (b) 4.32 wt % NCS, (c) 1.16 wt % N, (d) 1.65 wt % N, and (e) 2.32 wt % N.

absorption in the ultraviolet light region, expressed as the transmittance, decreasing from 30% (pure TiO_2) to 22 and 17% (λ = 387 nm) for the 2% $RuO_2-TiO_2$and 4% RuO_2-TiO_2 specimens, respectively. Moreover, the Ru-doped specimens developed apparent absorption red shifts. For instance, with the same transmittance of 30% as pure TiO_2, the spectrum of the 4% RuO_2-TiO_2 specimen (Figure 3c) shifts up to 500 nm, possibly because of the strong light absorbance of ruthenium oxide to the visible light.[29] In contrast, the low transmittance of Si,Te-doped TiO_2 specimen (Figure 4d) is mainly ascribed to the defused reflection of integrated $TiO_2-SiO_2-TeO_2$ nanotubes after chemical etching.[12]

Figure 5 demonstrates the transmission spectra of nanoporous TiO_2/Al_2O_3 films doped with nonmetallic elements, nitrogen, carbon, and sulfur. Similar to the ruthenium dopant, the enhancment of light absorption is also obtained for both NCS- and N-doped specimens, while with little dependence on the dopant concentration. Moreover, the N-doped specimens (parts c−e of Figure 5; doped with ammonia nitrate) enhance the light absorption of TiO_2 throughout the UV and visible light regions, whereas the NCS-doped specimen (Figure 5b; doped with thiourea) leads to a absorption mainly in the visible light region. Particularly, with the same transmittance of 28% as the pure TiO_2 (Figure 5a), the N-doped specimens develop an enhanced aborption red shift up to ≈580 nm.

3.4. Photocatalytic Activity in Decomposition of Acetaldehyde Gas. The photocatalytic activities of various TiO_2-based nanostructures doped with metal ions were evaluated by decomposing acetaldehyde under ultraviolet light irradiation according to the following reaction:[19]

$$2CH_3CHO + 5O_2 = 4CO_2 + 4H_2O \qquad (1)$$

For intuitional comparison of our results to the literature values, the most widely investigated (and probably the best) commercially available TiO_2 catalyst, Degussa P25, was also examined under the same experimental conditions. The yields and the concentrations of the produced CO_2 as a function of irradiation time for various samples

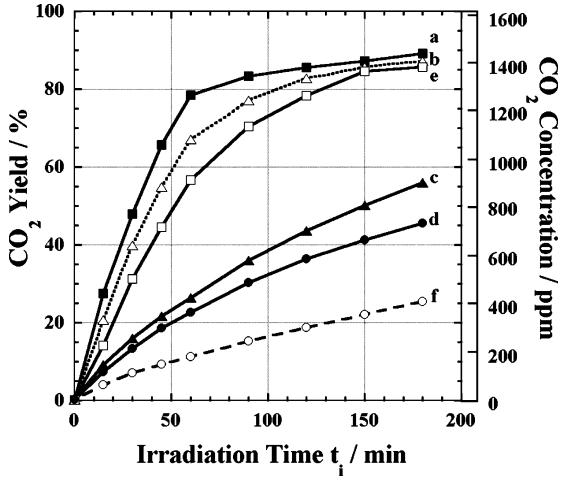

Figure 6. Time variations of yield and concentration of CO_2 produced by photodecomposition of acetaldehyde gas under ultraviolet light irradiation for composite nanoporous films coated with (a) pure TiO_2, (b) $TiO_2-SiO_2-TeO_2$, (c) TiO_2−2% RuO_2, (d) TiO_2−4% RuO_2, (e) an integrated array of $TiO_2-SiO_2-TeO_2$ nanotubules, and (f) commercial P-25 TiO_2 powder.

are shown in Figure 6. At the same irradiation time, all of the nanoporous specimens produced a much higher CO_2 yield or concentration than the P25, indicating the high photocatalytic performance of the formers. It should be pointed out here that, even though with similar apparent areas, i.e., 1.3 cm^2 (ϕ1.3 cm) for the powdery P25 and 1 cm^2 (1 × 1 cm) for the nanoporous samples, the really applicable surface areas of the nanoporous samples are actually smaller than that of P25, i.e., 1.0∼1.2 m^2 for the porous specimens (BET measurement) and 1.5 m^2 for the P25 (30 mg × 50 m^2/g).

The superior photocatalytic performences of the nanoporous samples to the P25 can be mainly attributed to the unique surface characteristics endowed by the highly porous structure. It can be reasonably decuced that the absorbability of acetaldehyde on nanoporous samples is higher than that on powdery P25, thus leading to a high photocatalytic activity.[40] The nanoporous structure with thin thickness (20−30 nm; Figure 1) may be benefit for enhancing the charge carrier separation [i.e., the generation of electron (e^-) and hole (h^+) pairs] in TiO_2 and/or inhibiting the recombination of the electron and hole pairs, which relates to high efficiency on photocatalysis. Moreover, a combination of the porous structure with open apertures/ordered straight channels and the appropriate transparence−absorbance of composite TiO_2/Al_2O_3 films on glass may also contribute to the high phtocatalytic activities of the nanoporous specimens. The porous structure provides fluent pathways to the reactant (acetaldehyde) and products (CO_2 and H_2O), thus enabling the effective utilization of the whole surface areas. In addition, the moderate transparence may allow for the UV light to reach the TiO_2 layer inside the nanopores in several micrometers thick and render an effective photodecomposition of the acetaldehyde absorbed there, thus leading to higher photocatalytic activities than the conventional powdery TiO_2.

The initial reaction rate (R_0) and quantum yield ($\Phi_{15\ min} = 5n_{CO_2}/n_{photon}$),[19] which are usually considered as the interpretation of photocatalytic activity, for the nanoporous specimens and P25 are listed in Table 1. For comparison, the ratios campared to the P25 sample are

(40) Li, D.; Haneda, H.; Hishida, S.; Ohashi, N. *Chem. Mater.* **2005**, *17*, 2596.

Table 1. Initial Reaction Rate (R_0) and Quantum Yield (Φ) of Various Nanoporous Samples for Decomposition of Acetaldehyde under Ultraviolet Light Irradiation

samples	$R_0/10^7$ (mol min^{-1})	Φ^a (%)
porous TiO_2	4.80 (12.97)[b]	18.35 (7.81)[b]
porous $TiO_2-SiO_2-TeO_2$	3.70 (10.0)	14.20 (6.04)
tubular $TiO_2-SiO_2-TeO_2$	2.97 (8.02)	10.42 (4.34)
porous TiO_2−2% RuO_2	0.95 (2.57)	10.42 (4.34)
porous TiO_2−4% RuO_2	0.86 (2.32)	10.42 (4.34)
powdery TiO_2 (P25)	0.37 (1)	2.35 (1)

[a] $\Phi = (5n_1)/n_2 \times 100\%$;[19] n_1 and n_2 are the numbers of CO_2 molecules produced at the reaction time of 15 min and the numbers of photons consumed on the catalyst surface, respectively; where the number of photons (n_2) = {light flux intensity (500 W/m^2)light wavelength (365×10^{-9} m)}/{Planck's constant (6.626×10^{-34} J s)light speed (2.998×10^8 m/s)} = 9.19×10^{18} (photon). [b] The values in parentheses are ratios compared to the value of the P25 sample.

also given in the table. Noticeably, the pure TiO_2-coated specimen exhibits the highest initial reaction rate and quantum yield of 4.80×10^{-7} mol/min and 18.35%, respectively, which are 13 times (in R_0) or 7.8 times (in $\Phi_{15\ min}$) higher than the P25, indicating the strikingly enhanced photocatalytic activity of the ordered, highly porous TiO_2 nanostructure on ITO/glass. This can be ascribed to the fact that the pure TiO_2 coating is composed of highly crystalline anatase with crystal sizes from 10 to 20 nm (Figure 3), which is thought to be the optimum grain size of anatase TiO_2 for high photocatalytic activity.[20,21] In contrast, the doping of metal ions (Ru, Si, and Te) leads to the decrease of the initial reaction rates, to a different extent, in the decomposition of acetaldehyde. Particularly, the Ru-doped TiO_2 specimens (lines c and d in Figure 6) exhibit low initial reaction rates that are nearly one-fifth of the pure TiO_2 sample. This may be ascribed to the inhibition effect of Ru-doping on the crystallization of TiO_2 (parts b and c of Figure 2) and/or the decrease of the transparency caused by the inclusion of RuO_2 (parts b and c of Figure 4). Moreover, increasing Ru dopant from 2 to 4% decreases the initial reaction rate from 0.95 to 0.86 ($\times 10^{-7}$ mol/min), which may be mainly ascribed to the lowering of the transmittance from ~20 to ~12% (λ = 387 nm). Nevertheless, owing to the absorption red shift to 500 nm (Figure 4c), the Ru-doped TiO_2 specimens with higher photocatalytic activities than the P25 may be applied as visible light photocatalysts for many pupposes.[29]

In addition, although they had similar transparency (parts a and d of Figure 4), the photocatalytic activity of Si,Te-doped TiO_2 specimen is slightly lower than that of the pure TiO_2, which can be mainly ascribed to the inhibition of glassy SiO_2-TeO_2 on the crystallization of anatase TiO_2.[11,12] Furthermore, the photocatalysis of integrated $TiO_2-SiO_2-TeO_2$ nanotubules on ITO/glass was also investigated (Figure 6e). Unexpectedly, the initial reaction rate is even lower than that in the nanoporous state (Figure 6b), although the surface area of integrated nanotubules would increase because of the exposure of the outer walls of the nanotubules. The decrease of the initial rate from nanoporous to nanotubular states for the $TiO_2-SiO_2-TeO_2$ specimens may be explained by the smoothing of the walls of the tubes because of the dissolution of tiny particles or nodules during the etching of the corrosive solution and/or the absorption of Cr^{6+} ions on the walls of the nanotubules, thus leading to the decreasing of the applicable area (the former) and/or the passivation (or poison) of photocatalytic TiO_2 (latter). Therefore, from the viewpoint of practical photocatalytic uses, the nanoporous composite films are preferable considering the aspects of mechanical strength and low-cost production.

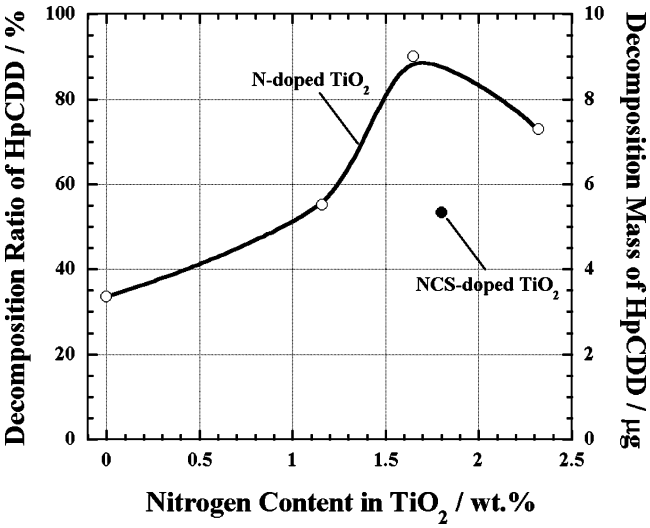

Figure 7. Decomposition ratios of a toxic dioxin (HpCDD) under ultraviolet light irradiation for nanoporous (N-doped TiO_2)/Al_2O_3 films on ITO/glass with different nitrogen concentrations.

3.5. Photodecomposition of Dioxins. The photocatalytic activities of the nanoporous N- and NCS-doped TiO_2/Al_2O_3 composite films on glass were investigated through photodecompositing (or photodegrading) a highly toxic dioxin, HpCDD, under ultraviolet light irradiation. Figure 7 displays the decomposition ratios of various TiO_2-coated nanoporous speciemens after UV irradiation for 7 h. The TiO_2-coated nanoporous specimens, both with and without doping, exhibit striking photocatalytic effects on the decomposition of the HpCDD under UV irradiation. Noticeably, the N-doped TiO_2 specimens lead to a remarkable enhanced effect on the photocatalysis compared to the pure TiO_2 specimen. Particularly, the speciemen containing 1.7 wt % nitrogen doped with ammonia nitrate exhibits the highest decomposition ratio ≈95%, which is reported by the present paper for the first time. Moreover, the NCS-doped TiO_2 specimens doped with thiourea (N content ≈ 1.65%) also shows an enhanced photocatalytic activity (decomposition ratio ≈ 53%) that is higher than the pure TiO_2 specimen (decomposition ratio ≈ 33%) but lower than the 1.7% N-doped specimen (95%). This indicates that the doping of carbon and sulfur in TiO_2 leads to an inhibiting effect on the photocatalysis under UV irradiation, which is different from the results under visible light irradiation.[36,37]

The enhanced photocatalytic activity of the doped TiO_2 in the decomposition of HpCDD may be explained from the basic principle of the photocatalytic reaction on TiO_2. Generally, electron (e^-) and hole (h^+) pairs are generated as ultraviolet light is irradiated on TiO_2. This produces powerful radical species that are capable of decomposing most organic compounds.[20] The photocatalytic decomposition reaction of HpCDD can be roughly expressed as the following reaction formula:

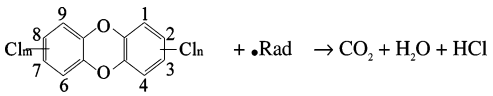

[2]

where •Rad is OH, HO_2, or NO_3 radicals.[41,42] The photo-

(41) Choi, W.; Hong, S. J.; Chang, Y. S.; Cho, Y. *Environ. Sci. Technol.* **2000**, *34*, 4810.

catalytic decomposition of HpCDD on TiO_2 is described by the first-order reaction kinetics with a half-life of 3.9 h, initiated by OH radical attack, without formation of stable intermediates or dechlorinated PCDDs.[41] In the present study, the enhanced photocatalytic activity of the N-doped nanoporous TiO_2/Al_2O_3 films on glass can be ascribed to several factors. First, the enhancement of light absorption throughout the UV and visible light regions (Figure 5) for the N-doped TiO_2 specimens leads to effective photocatalytic reactions under the irradiation with a relatively low light intensity (i.e., 0.8 mW/cm^2). Second, the band-cap narrowing effect because of the nitrogen doping contributes the high photocatalytic decomposition of HpCDD on N-doped TiO_2 specimens. According to J. Premkumar,[34] the doping of nitrogen in TiO_2 leads to a band-cap narrowing from 3.1 to 2.8 eV, caused by the shifting of the top edge of the valance band to the negative direction because of the mixing of N 2p and O 2p states and the shifting of the bottom edge of the conduction band to the positive direction because of the generation of oxygen vacancies. This definitely decreases the energy rampart that must be overcome to produce powerful radical species, thus increasing the ratios or numbers of active radicals and enhancing the decomposition of HpCDD under UV irradiation. Furthermore, the substitution of oxygen by nitrogen in the N-doped TiO_2 specimens may produce more oxygen vacancies that may, in turn, enhance the charge carrier separation/transportation in TiO_2 and/or inhibit the recombination of electron and hole pairs, thus leading to a high photocatalytic capability. Therefore, the fact that the 1.7% N−TiO_2 specimen doped with ammonia nitrate developed the highest photocatalytic effect (decomposition ratio) may reflect the optimum combination of band-cap narrowing, light absorption, and the charge carrier separation/transportation. In contrast, the explanation on photocatalytic behavior of the NCS-doped TiO_2 specimen may be more complicated. It may be ascribed to the relatively low absorbance (Figure 5b) and/or the chemical states of carbon and sulfur elements in TiO_2,[36] which is no longer elaborated in the present paper.

(42) Lee, J. E.; Choi, W. Y.; Mhin, B. J.; Balasubramanian, K. *J. Phys. Chem. A* **2004**, *108*, 607.

Conclusions

We successfully fabricated various ordered, nanoporous TiO_2/Al_2O_3 composite films doped with metal elements (Ru, Si, and Te) and nonmetal elements (N, C, and S) directly on ITO/glass substrates. The nanoporous pristine TiO_2/Al_2O_3 film exhibited the highest photocatalytic activity in decomposing acetaldehyde under UV irradiation, which is 13 times in initial reaction rate or 7.8 times in quantum yield higher than the best commercially available TiO_2 material, Degussa P25. To the best of our knowledge, it is the highest value of photocatalytic activity for the pristine TiO_2 nanostructures under UV irradiation that has been reported thus far. Moreover, it is confirmed for the first time that the nanoporous TiO_2/Al_2O_3 films with nitrogen dopant possess remarkable photocatalysis in decomposing a highly toxic dioxin, HpCDD, under UV irradiation. Particularly, the N-doped TiO_2 nanoporous film containing 1.7 wt % nitrogen exhibited a high decomposition ratio ≈95%, showing a promising future for practical uses in circumstance cleaning. Furthermore, owing to the enhanced absorption red shift, the N- or Ru-doped TiO_2/Al_2O_3 films on ITO/glass may be also utilized as visible light photocatalysts for multifunctional applications such as atmosphere cleaning, water purification, and solar-energy cells, which are being explored.

Acknowledgment. This work is part of the Millennium Project of "Exploration and Creation of a Catalyst for Removing Harmful Chemical Substances", which was sponsored by the Ministry of Education, Culture, Sports, Science, and Technology of Japan.

LA050902J